Supplementary Material for "Coherent Spins in van der Waals Semiconductor GeS_2 at Ambient Conditions"

Sumukh Vaidya,[†] Xingyu Gao,[†] Saakshi Dikshit,[‡] Zhenyao Fang,[¶] Andres E Llacsahuanga Allcca,[†] Yong P Chen,[†,‡,§,‖] Qimin Yan,[¶] and Tongcang Li[*,†,‡,§,‖]

[†]*Department of Physics and Astronomy, Purdue University, West Lafayette, Indiana 47907, USA*

[‡]*Elmore Family School of Electrical and Computer Engineering, Purdue University, West Lafayette, Indiana 47907, USA*

[¶]*Department of Physics, Northeastern University, Boston, Massachusetts 02115, USA*

[§]*Purdue Quantum Science and Engineering Institute, Purdue University, West Lafayette, Indiana 47907, USA*

[‖]*Birck Nanotechnology Center, Purdue University, West Lafayette, Indiana 47907, USA*

E-mail: tcli@purdue.edu

Sample Preparation

We purchased commercially available β-GeS_2 crystals from Ossila. These are then tape exfoliated and transferred to Si/SiO_2 substrates and annealed in air at 450 ^{o}C for 2 hours. Then, using a polymer based transfer method they are transferred to a gold microwave stripline fabricated on Sapphire. We perform Raman spectroscopy measurements of the sample on gold to confirm the presence of β-GeS_2 in the sample and observe sharp peaks at 360 cm^{-1} as seen in Figure S.1(a).[1,2] This confirms that the material is β-GeS_2. During the course of sample preparation and measurements, we found that some crystals labeled and sold commercially as β-GeS_2 were actually GeS. We performed our measurements after confirmation of the Raman spectra, and suggest that others do the same to ensure the material is correct. The two materials can be distinguished by color as well. GeS is a dark colored crystal on account of its smaller bandgap (1.6 eV), whereas β-GeS_2 is a white-transparent crystal as seen in main text Fig 1(b) and Fig S.1(b). Both materials can be tape exfoliated and transferred via the polymer transfer method. We measure the thickness of the flakes to be of the order of tens nanometers, as seen in Fig S.2.

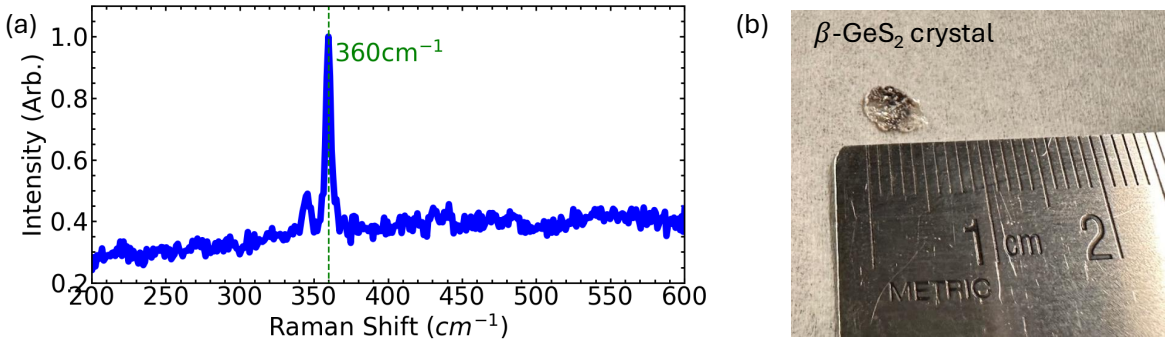

Figure S.1: (a) Raman spectrum of the β-GeS_2 on a gold substrate. The vertical line is 360 cm^{-1}, confirming that the sample is β-GeS_2. (b) Image of a β-GeS_2 crystal next to a ruler.

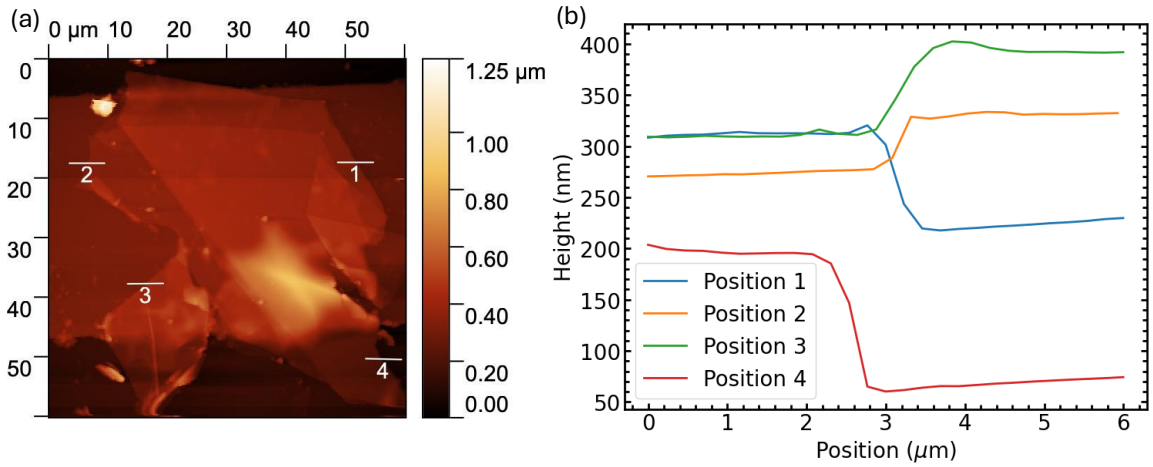

Figure S.2: (a)AFM measurement of the sample used in experiments. The markers describe the cross sections as measured in (b). (b) Cross section profiles of the flake. Typical flake thickness is tens of nanometers.

Experimental Setup

The sample is loaded into a custom built confocal microscopy setup, where it is excited by green laser light of wavelength 532 nm and power 300 μW - 1 mW. An Olympus Objective lens (MPlanFL 100x) of NA 0.9 is used to focus the laser and collect the emission from the sample. The emission is filtered by a 550 nm longpass filter and sent to an Excelitas Single Photon Counting Module (SPCM) through a multimode optic fiber. The microwaves (MW) are supplied by a function generator (Stanford Research Systems SG386) and sent through an MW amplifier . A Swabian Instruments Pulse Streamer 8/2 is used to setup and synchronize all the pulses in the experiment and MW switches are used to modulate all the pulsed signals.For the pulsed experiments, we use IQ modulation using an arbitrary waveform generator (Zurich Instruments HDAWG) to get high precision arbitrary waveforms. A National Instruments FPGA (NI 7855) is used to count the incoming pulses from the SPCM and calculate the contrast under the various measurement schemes.

g-factor Measurement

We vary the external magnetic field by moving the position of the external permanent magnet and sweep the frequency to measure the ODMR contrast peaks for different magnetic fields. These are then fit to a Lorentzian function to find the peak frequency. To calibrate the magnetic field for each position of the permanent magnet, we perform the same experiment for a known spin-1/2 carbon related defect sample in hBN. Using this sample the magnetic field for each position is measured and the peak positions for the β-GeS_2 are then plotted against the field value, as seen in Fig S.3. This is then fit to a linear function to obtain a slope and calculate the g-factor for the β-GeS_2 spin defects, as shown in main text Figure 1(f).

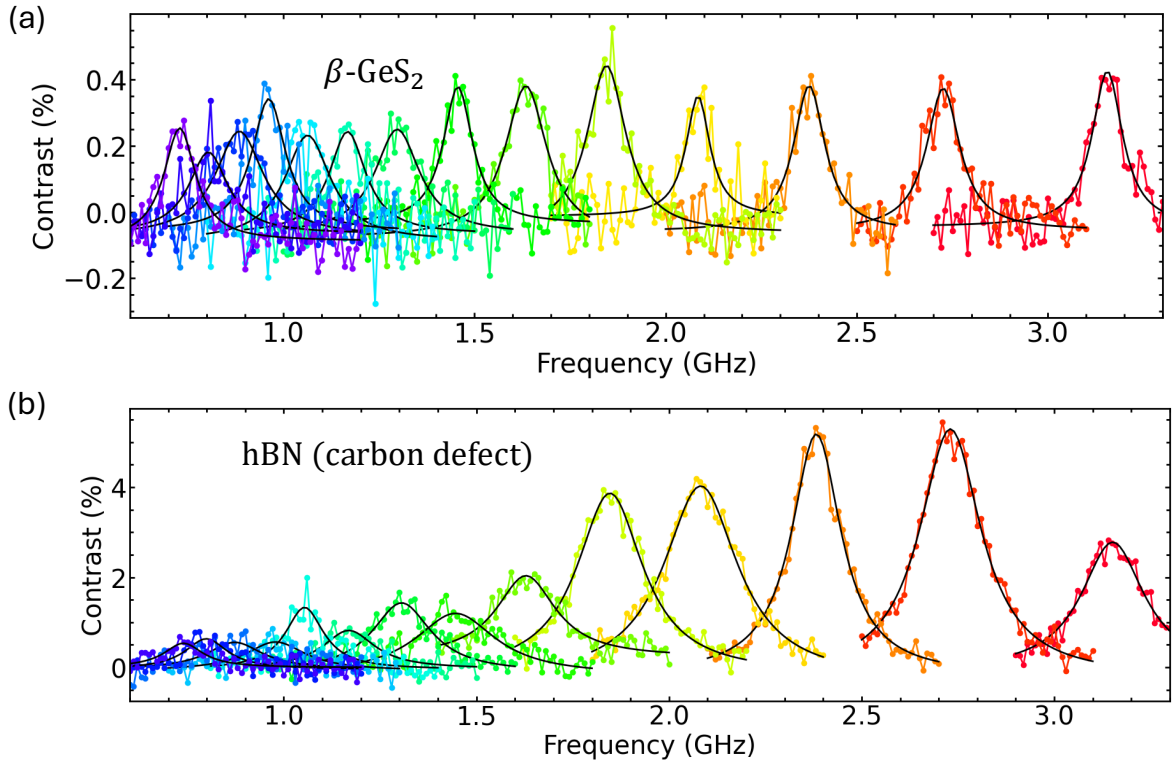

Figure S.3: (a) Measurement of the β-GeS_2 ODMR contrast at various external magnetic fields. (b) Measurement of hBN carbon related spin defects contrast at the same magnet position to determine the g-factor.

Spin-Pair Modeling

We use the Lindblad Master Equation formalism to calculate the state dynamics as described elsewhere.[3,4] The master equation is given by

$$\dot{\rho}(t) = -\frac{i}{\hbar}[H, \rho(t)] + \sum_k \Gamma_k (L_k \rho(t) L_K^\dagger - \frac{1}{2}\{L_k^\dagger L_k, \rho(t)\}) \tag{1}$$

Here $\rho(t)$ denotes the time dependent density matrix, H is the system Hamiltonian, [ ] denotes the commutator, Γ_k is the rate of the k^{th} decoherence process, L_k is the k^{th} Lindblad collapse operator and {} is the anticommutator. This equation governs the time evolution of a system's density matrix under a Hamiltonian and other nonunitary decoherence processes. We use the Python toolbox QuTiP[5] to simulate the system dynamics. Assuming a 3-level system with states $|0\rangle, |1\rangle$ and $|2\rangle$, with $|0\rangle$ being the pure singlet state and $|1\rangle, |2\rangle$ being the states in the triplet configuration, we use the initial state under laser polarization as $|1\rangle$. The system Hamiltonian is given by

$$H = \begin{bmatrix} 0 & 0 & 0 \\ 0 & -\Delta/2 & \Omega/2 \\ 0 & \Omega/2 & \Delta/2 \end{bmatrix} \tag{2}$$

where Ω is the frequency of the coherent drive and Δ is the energy level separation between the states $|1\rangle, |2\rangle$. Each of the Lindblad operators are given by $|i\rangle\langle j|$. Γ_{10} and Γ_{20} are the decay rates from $|1\rangle, |2\rangle$ to $|0\rangle$ and Γ_{12} is the dephasing rate between $|1\rangle$ and $|2\rangle$.

This system is then solved and the populations are calculated. Under the Rabi drive, the populations between the states are driven coherently and undergo time evolution as governed by the Lindblad equation. Assuming each state has different PL emission under laser excitation, we simulate the total emission as

$$I = \alpha_0 \rho_{00} + \alpha_1 \rho_{11} + \alpha_2 \rho_{22} \tag{3}$$

where $\alpha_{0,1,2}$ are free parameters fit to the data as described in Figure 2(a) in the main text. Their ratios are $\alpha_1/\alpha_0 \lesssim 0.99$ and $\alpha_2/\alpha_0 \lesssim 0.2$. α_0 is then freely fit to match the scale of magnitude of Rabi oscillations.

Polarization dependence of ODMR contrast

To probe if the PL emission has a polarization dependence indicating some symmetry in the emitters, we use both linear and circular polarization at different angle to see how it affects the ODMR contrast as shows in Figure S.4. We see some trends in the polarization with the angle of the polarizer, but due to low contrast and noise in the measurements it is not easy to draw any meaningful conclusions about the polarization dependence of the ODMR contrast. Also since these defects are expected to be ensemble emitters, it is not expected that their emissions will show polarization dependence on the polarization.

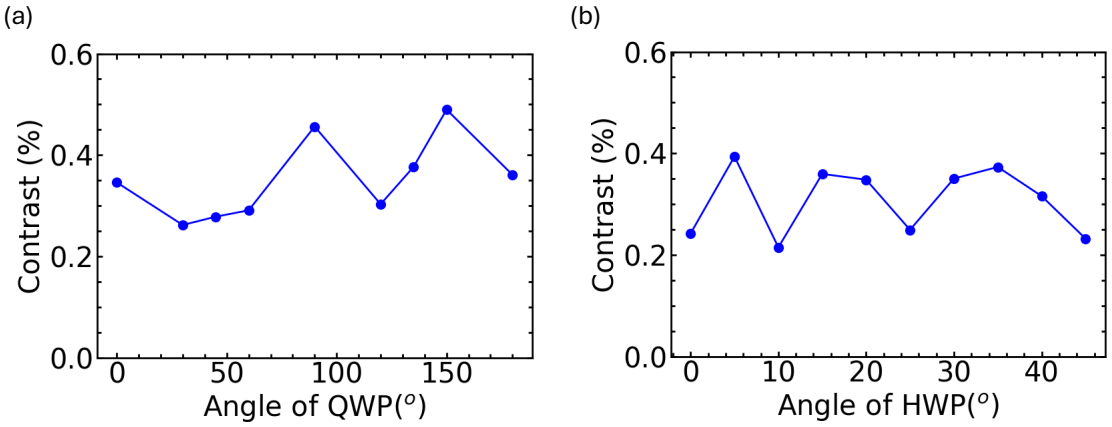

Figure S.4: Polarization dependence of ODMR contrast. (a) Linear polarization dependence with the axis of the quarter wave plate. (b) Dependence on circular polarization with the angle of the half wave plate.

Thermal annealing effects on β-GeS_2

During the preparation of samples used in this paper we performed thermal annealing of β-GeS_2 samples at 450 ^{o}C for up to 24 hours at room pressure in both vacuum and at ambient pressure. We observed that under vacuum pumping and high temperature the β-GeS_2 breaks down and disappears within our annealing duration of 2 hours. When performed at ambient pressure the annealing yields some flakes that can be transferred and used for our experiments. Annealing at 500 ^{o}C causes the samples to disappear at both vacuum and ambient pressure. This suggests that this temperature range (400-500 ^{o}C) is close to the breakdown temperature of the material and the ambient pressure has a role to play in whether the samples survive the annealing. Flakes annealed for 24 hours look damaged under the microscope and are in general much more difficult to transfer to the gold stripline waveguide, as compared to fresh or 2 hour annealed flakes. The Raman signal from the flakes becomes weaker with increased annealing time. Some thinner flakes lose all Raman signature around 360 cm^{-1} entirely, suggesting the breakdown of the material of the flake. Figures S3 shows the Raman spectra and microscope images of some flakes on Si/SIO_2 substrates as a function of annealing time.

Stability under immersion in water

Some sulfides are expected to be unstable in air due to reaction with atmospheric humidity and hence are unsuitable for long term experimentation under ambient conditions. We subjected the β-GeS_2 samples to water immersion during sample preparation and observed that water does not seem to affect the samples. β-GeS_2 seems to be stable under water for 1 hour, with the flakes showing no discernible change before and after water immersion. The Raman signal as shown in Figure S.4 a,b is also unchanged, suggesting that the material is stable when immersed in water.

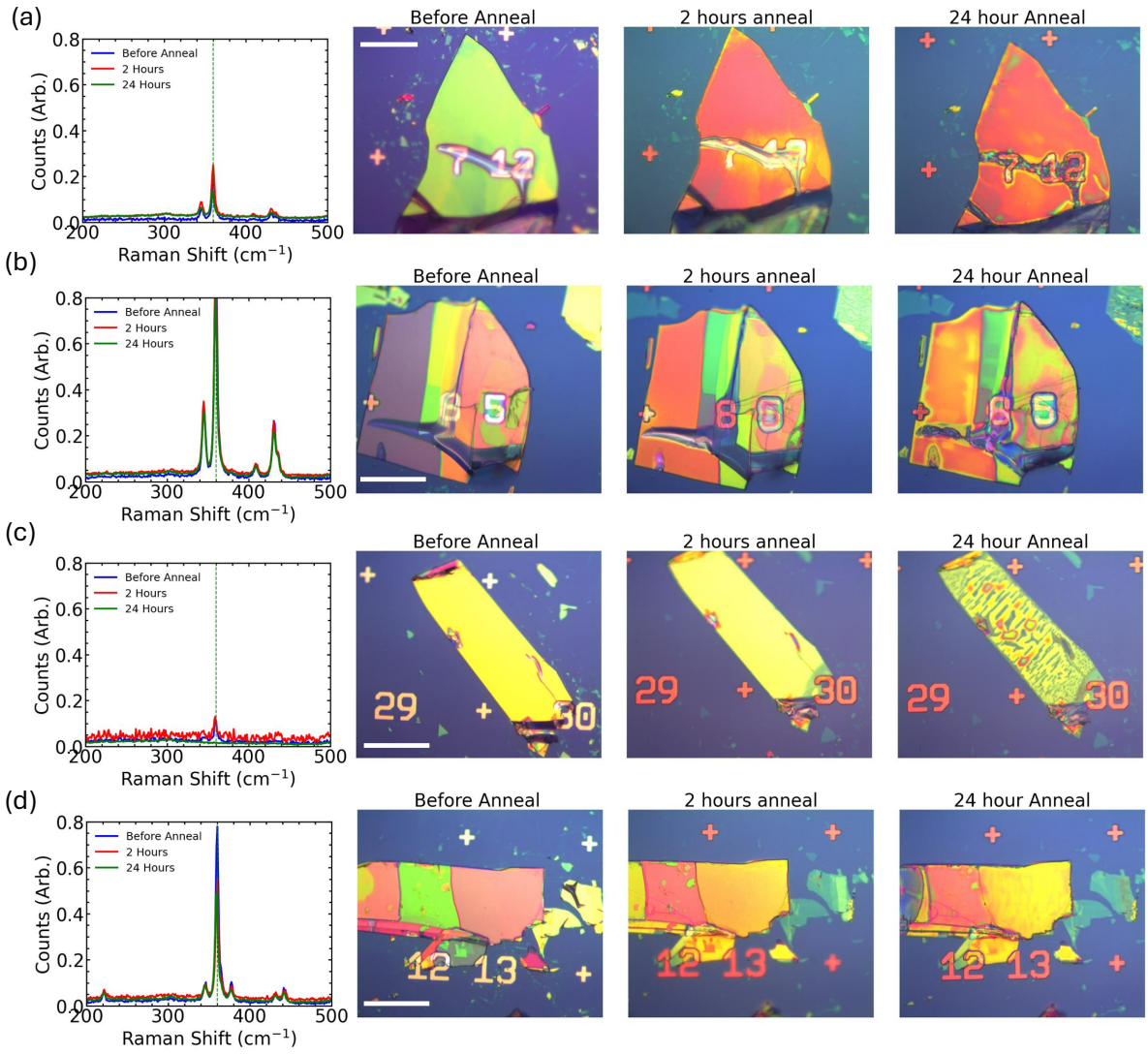

Figure S.5: (a),(b),(c),(d) Effect of thermal annealing at 450 ^{o}C for 2 hours and 24 hours on freshly exfoliated β-GeS_2 samples. With time the flakes are seen to be damaged and stick more strongly to the Si/SiO_2 substrates. The scale bar is 50 μm.

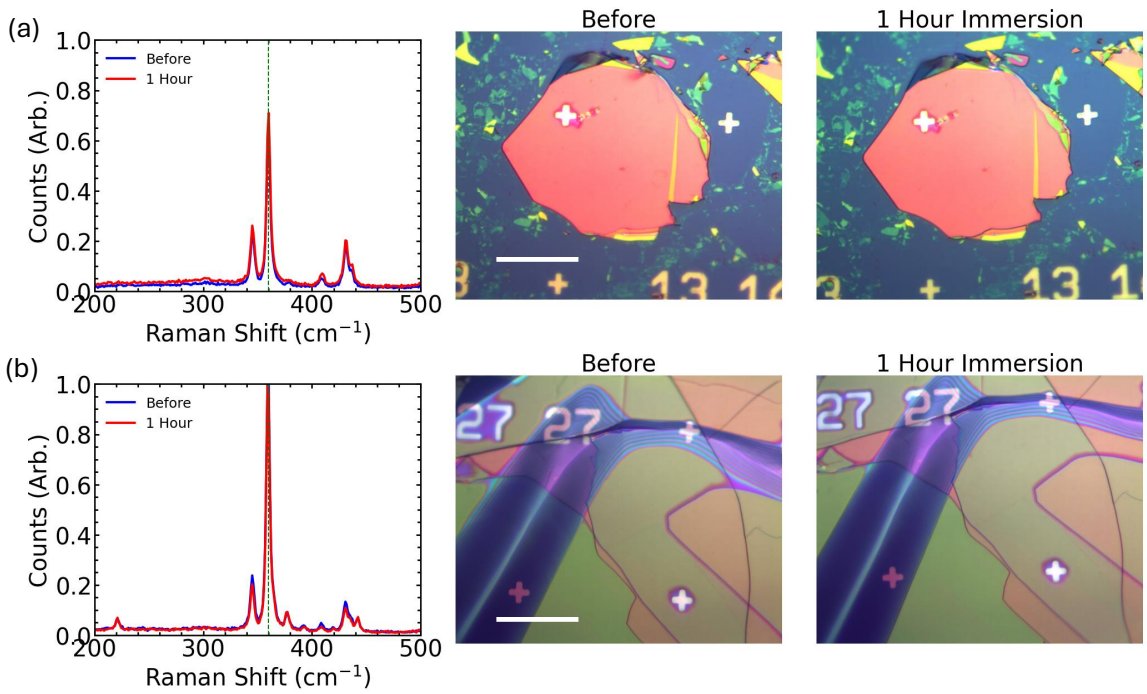

Figure S.6: (a),(b) Effect of water immersion for 1 hour on freshly exfoliated β-GeS_2 samples. With time the flakes are seen to be unchanged and the Raman signal remains the same. The scale bar is 50 μm.

DFT Methods

Density functional theory (DFT) calculations were performed using the Vienna Ab initio Simulation Package (VASP).[6,7] We adapted the projector-augmented wave (PAW) pseudopotentials[8] and HSE06 hybrid functional[9] for all calculations. For all calculations, the energy convergence threshold of 10^{-7} eV and a vacuum level of 20 Å are used, and for structural relaxation calculations, the force convergence threshold is 0.005 eV/Å. The DFT-D3 correction scheme is also included to capture the van der Waals interactions.[10] For defect property calculations, the 2×1×1 supercell is adopted, and the defect formation energy $E^f[X^q]$ for the defect X in charge state q is defined as[11]

$$E^f[X^q] = E[X^q] - E[bulk] + \Sigma_i[n_i\mu_i] + q(E_F + E_\nu) + \Delta E_{corr}$$

where $E[X^q]$ and E[bulk] are the total energies of the defective supercell and the pristine supercell, μ_i represents the chemical potential for the chemical species i which is calculated from the elemental bulk crystal, E_ν is the valence band maximum, and ΔE_{corr} is the charge correction used for correcting the electrostatic interactions between charged images and the supercell effect. In this work, we used the Freysoldt Neugebauer charge-correction scheme, implemented in the package sxdefectalign2d[12] to calculate the correction term.

References

(1) Mitsa, V.; Holomb, R.; Lovas, G.; Veres, M.; Ivanda, M.; Kovach, T. Spectroscopic evidence of coexistence of clusters based on low (α) and high temperature (β) GeS 2 crystalline phases in glassy germanium disulfide matrix. 2014 37th International Convention on Information and Communication Technology, Electronics and Microelectronics (MIPRO). 2014; pp 7–10.

(2) Yang, Y.; Liu, S.-C.; Wang, X.; Li, Z.; Zhang, Y.; Zhang, G.; Xue, D.-J.; Hu, J.-S. Polarization-sensitive ultraviolet photodetection of anisotropic 2D GeS2. *Advanced Functional Materials* **2019**, *29*, 1900411.

(3) Robertson, I. O.; Whitefield, B.; Scholten, S. C.; Singh, P.; Healey, A. J.; Reineck, P.; Kianinia, M.; Barcza, G.; Ivády, V.; Broadway, D. A.; Aharonovich, I.; Tetienne, J.-P. A charge transfer mechanism for optically addressable solid-state spin pairs. *arXiv preprint arXiv:2407.13148* **2024**,

(4) Gao, X.; Vaidya, S.; Li, K.; Ge, Z.; Dikshit, S.; Zhang, S.; Ju, P.; Shen, K.; Jin, Y.; Ping, Y.; Li, T. Single nuclear spin detection and control in a van der Waals material. *Nature* **2025**, *643*, 943.

(5) Lambert, N. et al. QuTiP 5: The Quantum Toolbox in Python. 2024; `https://arxiv.org/abs/2412.04705`.

(6) Kresse, G.; Hafner, J. Ab initio molecular dynamics for liquid metals. *Physical review B* **1993**, *47*, 558.

(7) Kresse, G.; Furthmüller, J. Efficiency of ab-initio total energy calculations for metals and semiconductors using a plane-wave basis set. *Computational materials science* **1996**, *6*, 15–50.

(8) Kresse, G.; Joubert, D. From ultrasoft pseudopotentials to the projector augmented-wave method. *Physical review b* **1999**, *59*, 1758.

(9) Krukau, A. V.; Vydrov, O. A.; Izmaylov, A. F.; Scuseria, G. E. Influence of the exchange screening parameter on the performance of screened hybrid functionals. *The Journal of chemical physics* **2006**, *125*, 224106.

(10) Grimme, S.; Ehrlich, S.; Goerigk, L. Effect of the damping function in dispersion corrected density functional theory. *Journal of computational chemistry* **2011**, *32*, 1456–1465.

(11) Van de Walle, C. G.; Neugebauer, J. First-principles calculations for defects and impurities: Applications to III-nitrides. *Journal of applied physics* **2004**, *95*, 3851–3879.

(12) Freysoldt, C.; Neugebauer, J. First-principles calculations for charged defects at surfaces, interfaces, and two-dimensional materials in the presence of electric fields. *Physical Review B* **2018**, *97*, 205425.